

## Chapter 2

# Finite Element in Manufacturing Processes

**Abstract** This chapter explains the basis of the finite element method, highlighting the application for manufacturing modeling problems. A review of the principles of plasticity, as used in modeling of machining and forming processes is presented, including the most frequently used constitutive models. The key issues of the finite element method modeling of these mechanical processes are also explained according with the last researches in this field.

### 2.1 Basis of the Finite Element Method

The finite element method (FEM) has gained popularity in the last years as a powerful numeric method for finding good approximate solutions for systems of partial differential equations. This method is especially suitable when the problem is defined over geometrically complex spatial domains. For this reason, the FEM has been successfully applied to a wide field of engineering problems, such as mechanics of materials (elastic and non-elastic), fluid dynamics, heat transfer and electromagnetism.

The FEM aims to solve a differential equation set:

$$\mathbf{A}(\mathbf{u}) = [A_1(\mathbf{u}), A_2(\mathbf{u}), \dots]^T = \mathbf{0}; \quad (2.1a)$$

in a domain  $\Omega$  (see Fig. 2.1), being  $\mathbf{u}$  the unknown state variable; together with the boundary conditions:

$$\mathbf{B}(\mathbf{u}) = [B_1(\mathbf{u}), B_2(\mathbf{u}), \dots]^T = \mathbf{0}; \quad (2.1b)$$

on the boundary,  $\Gamma$ , of the domain. In these equations,  $A_i(\bullet)$  and  $B_i(\bullet)$  are differential operators.

**Fig. 2.1** Domain and boundary of a problem

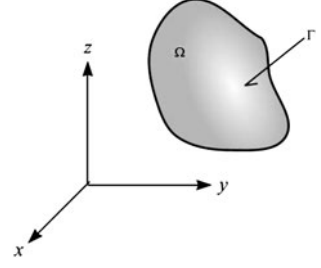
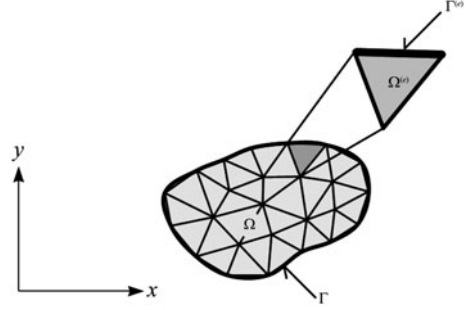


**Fig. 2.2** Element domain and boundary



The central idea of the FEM is to replace the exact solution,  $\mathbf{u}$ , by an approximation,  $\mathbf{u}^*$ , of the form:

$$\mathbf{u} \approx \mathbf{u}^* = \sum_{i=1}^n \mathbf{N}_i \mathbf{a}_i = \mathbf{N} \mathbf{a}; \quad (2.2)$$

where  $\mathbf{N}_i$  are the shape functions, predefined in terms of the independent variables (usually, the coordinates,  $\mathbf{x}$ ) and  $\mathbf{a}_i$  are parameters, initially unknown, which should be determined as a result of the application of the method.

In order to obtain this solution, the Eqs. (2.1a, b) must be combined in the so-called weak form:

$$\int_{\Omega} \mathbf{G}_j(\mathbf{u}^*) d\Omega + \int_{\Gamma} \mathbf{g}_j(\mathbf{u}^*) d\Gamma = \mathbf{0} \quad j = 1 \dots n; \quad (2.3)$$

which permits the approximation to be obtained for every portion of the domain and assembled (Fig. 2.2):

$$\sum_{e=1}^m \int_{\Omega^{(e)}} \mathbf{G}_j(\mathbf{u}^*) d\Omega + \int_{\Gamma^{(e)}} \mathbf{g}_j(\mathbf{u}^*) d\Gamma = \mathbf{0} \quad j = 1 \dots n; \quad (2.4)$$

where  $\Omega^{(e)}$  is the domain of the  $e$ th portion and  $\Gamma^{(e)}$  its part of the boundary (Zienkiewicz and Taylor 2000).

These portions are known as elements and usually have a simple geometric shape. Depending on the domain, there are elements with different dimensionality. For example, a bar (Fig. 2.3a) is a typical one-dimensional element; triangles

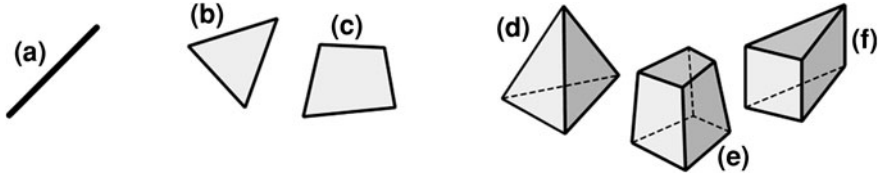


**Fig. 2.3** Types of elements **a** Bar element. **b** Triangular element. **c** Quadrangular element. **d** Tetrahedral element. **e** Hexahedral (brick) element. **f** Pentahedral (wedge) element

(Fig. 2.3b) and quadrilaterals (Fig. 2.3c) are the most common two-dimensional elements; and, finally, tetrahedrons (Fig. 2.3d), hexahedrons (Fig. 2.3e) and wedges (Fig. 2.3f) are widely used for meshing three-dimensional domains.

If the differential equations are linear, that is, if the Eq. (2.1a, b) can be written in the form:

$$\begin{aligned} \mathbf{A}(\mathbf{u}) &= \mathbf{L}\mathbf{u} + \mathbf{p} = \mathbf{0} \quad \text{in } \Omega, \\ \mathbf{B}(\mathbf{u}) &= \mathbf{M}\mathbf{u} + \mathbf{q} = \mathbf{0} \quad \text{on } \Gamma; \end{aligned} \quad (2.5)$$

then, the approximating equation system (2.4) yields a set of linear algebraic equations of the form:

$$\mathbf{K}\mathbf{a} + \mathbf{f} = \mathbf{0}; \quad (2.6)$$

with

$$\mathbf{K}_{ij} = \sum_{e=1}^m \mathbf{K}_{ij}^{(e)} \quad \text{and} \quad \mathbf{f}_{ij} = \sum_{e=1}^m \mathbf{f}_{ij}^{(e)}; \quad (2.7)$$

which can be numerically solved.

There are two main approaches for obtaining the weak formulation in the FEM; they are the functional variational principle and the weighted residual method.

The essence of the variational method is to calculate the total potential,  $\Pi$ , also known as the functional of the system and, then, to consider the stationarity of this total potential:

$$\delta \Pi = 0; \quad (2.8)$$

as an equilibrium condition (Bathe 1996).

On the other hand, the weighted residual method is based on considering that from the (Eq. 2.1a, b) it follows that:

$$\int_{\Omega} \mathbf{v}_j^T \mathbf{A}(\mathbf{N}\mathbf{a}) \, d\Omega + \int_{\Gamma} \mathbf{w}_j^T \mathbf{B}(\mathbf{N}\mathbf{a}) \, d\Gamma = \mathbf{0}, \quad j = 1 \dots n; \quad (2.9)$$

where  $\mathbf{A}(\mathbf{N}\mathbf{a})$  and  $\mathbf{B}(\mathbf{N}\mathbf{a})$  represent the residual errors of replace the approximate solution in the differential equation set and in the boundary conditions, respectively, and  $\mathbf{v}_j$  and  $\mathbf{w}_j$  are some weighting functions. In the Galerkin method,

$\mathbf{v}_j = \mathbf{w}_j = \mathbf{N}_j$ , i.e., the original shape functions are used as weighting (Zienkiewicz and Taylor 2000).

## 2.2 FEM for Linear Elastostatic Problems

The basic application of the FEM in structural mechanics is in linear elastostatic problems, where on the domain,  $\Omega$ , there are three unknown fields: the displacement field,  $\mathbf{u} = [u_x, u_y, u_z]^T$ ; the strains field,  $\boldsymbol{\varepsilon} = [\varepsilon_{xx}, \varepsilon_{yy}, \varepsilon_{zz}, \varepsilon_{yz}, \varepsilon_{xz}, \varepsilon_{xy}]^T$ ; and the stress field,  $\boldsymbol{\sigma} = [\sigma_{xx}, \sigma_{yy}, \sigma_{zz}, \sigma_{yz}, \sigma_{xz}, \sigma_{xy}]^T$ . As result of the load conditions of the domain, the body force,  $\mathbf{b} = [b_x, b_y, b_z]^T$ , is known on the entire domain. Moreover, at some portion,  $\Gamma_u$ , of the boundary, the values of the displacements are prescribed as equal to  $[\mathbf{u}]$ , and, at other portion,  $\Gamma_t$ , the values of the tractions are also prescribed as equal to  $[\mathbf{t}]$  (see Fig. 2.4). These relationships are known as boundary conditions. The boundary portions must fulfill the conditions:

$$\Gamma_u \cup \Gamma_t = \Gamma \quad \text{and} \quad \Gamma_u \cap \Gamma_t = \emptyset \quad (2.10)$$

A set of equations establishes the relationships between the different variables defined for the problem. The first one is the cinematic equation, which relates the displacements and strains in the entire domain:

$$\boldsymbol{\varepsilon} = \nabla_s \mathbf{u}; \quad (2.11a)$$

where  $\nabla_s$  represents the symmetric matrix gradient operator:

$$\nabla_s = \begin{bmatrix} \partial/\partial x & 0 & 0 & 0 & \partial/\partial z & \partial/\partial y \\ 0 & \partial/\partial y & 0 & \partial/\partial z & 0 & \partial/\partial x \\ 0 & 0 & \partial/\partial z & \partial/\partial y & \partial/\partial x & 0 \end{bmatrix}^T \quad (2.11b)$$

On the other hand, the equilibrium equation:

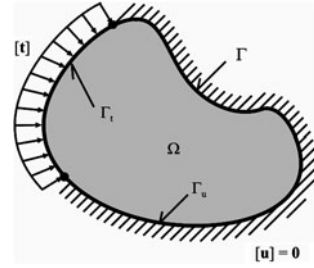
$$\nabla_s^T \boldsymbol{\sigma} + \rho \mathbf{b} = \mathbf{0}; \quad (2.12)$$

establishes the relationships between the body force and the stress field, and it is the application of the principle of conservation of lineal momentum. Finally, the constitutive equation relates the strain and stress fields. This is particular of every material at every specific condition. For linear elastic materials, this constitutive equation is given by the generalized Hooke's law:

$$\boldsymbol{\sigma} = \mathbf{C}^E \boldsymbol{\varepsilon}; \quad (2.13a)$$

where  $\mathbf{C}^E$  is the tensor of elasticity, which can be written in matrix form as:

**Fig. 2.4** Domain and boundary definitions



$$\mathbf{C}^E = \begin{bmatrix} c_{11} & c_{12} & c_{13} & c_{14} & c_{15} & c_{16} \\ & c_{22} & c_{23} & c_{24} & c_{25} & c_{26} \\ & & c_{33} & c_{34} & c_{35} & c_{36} \\ & & & c_{44} & c_{45} & c_{46} \\ & \text{sym.} & & & c_{55} & c_{56} \\ & & & & & c_{66} \end{bmatrix} \quad (2.13b)$$

In the special case of homogeneous and isotropic materials, the matrix of elasticity can be reduced to:

$$\mathbf{C}^E = \frac{E}{(1-2\nu)(1+\nu)} \begin{bmatrix} 1-\nu & \nu & \nu & 0 & 0 & 0 \\ & 1-\nu & \nu & 0 & 0 & 0 \\ & & 1-\nu & 0 & 0 & 0 \\ & & & 1-2\nu & 0 & 0 \\ & \text{sym.} & & & 1-2\nu & 0 \\ & & & & & 1-2\nu \end{bmatrix}; \quad (2.13c)$$

being  $E$ , the Young's modulus and  $\nu$ , the Poisson's ratio of the material.

Additionally, from the definition of stress tensor is obtained the relationship that links the stress fields and the prescribed tractions, on the portion of the boundary,  $\Gamma_u$ , where these tractions act:

$$\mathbf{n}\sigma = [\mathbf{t}]; \quad (2.14a)$$

where

$$\mathbf{n} = \begin{bmatrix} n_x & 0 & 0 & 0 & n_z & n_y \\ 0 & n_y & 0 & n_z & 0 & n_x \\ 0 & 0 & n_z & n_y & n_x & 0 \end{bmatrix} \quad (2.14b)$$

and  $n_x$ ,  $n_y$  and  $n_z$  are the components of the outward normal on the boundary.

This set of equations form the so-called strong formulation of the linear elastostatics, and can be represented, in a very convenient way by using the popular Tonti diagram, as shown in Fig. 2.5.

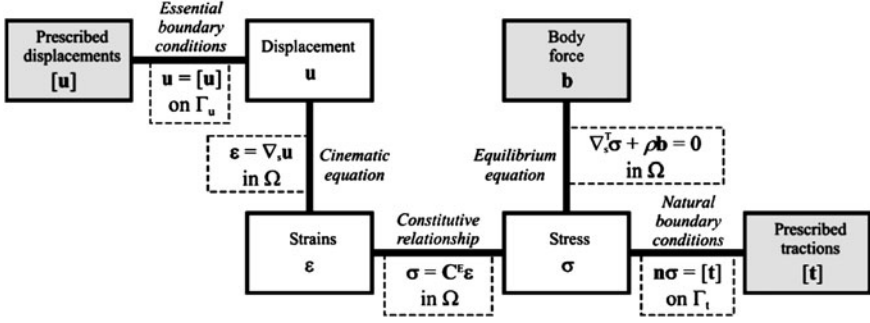


Fig. 2.5 Tonti diagram for the strong form of linear elastostatics

In order to solve this kind of problem by applying the FEM, the strong formulation is replaced by the weak formulation. This enforces the relationships in an integral sense rather than point by point. In elastostatics applications, this weak formulation is given by the Hamilton's principle:

$$\delta \int_{t_1}^{t_2} L \, dt = 0; \quad (2.15)$$

where the Lagrangian functional,  $L$ , is computed as:

$$L = T - U + W; \quad (2.16)$$

and the kinetic energy,  $T$ , the internal energy (here, the elastic strain energy),  $U$ , and the work done by the external forces,  $W$ , can be defined in the integral forms (Liu and Quek 2003):

$$T = \frac{1}{2} \int_{\Omega} \rho \dot{\mathbf{u}}^T \dot{\mathbf{u}} \, d\Omega; \quad (2.17a)$$

$$U = \frac{1}{2} \int_{\Omega} \boldsymbol{\varepsilon}^T \boldsymbol{\sigma} \, d\Omega = \frac{1}{2} \int_{\Omega} \boldsymbol{\varepsilon}^T \mathbf{C}^E \boldsymbol{\varepsilon} \, d\Omega; \quad (2.17b)$$

$$W = \int_{\Omega} \mathbf{u}^T \mathbf{b} \, d\Omega + \int_{\Gamma_t} \mathbf{u}^T \mathbf{t} \, d\Gamma. \quad (2.17c)$$

As the problem is static, the Hamilton principle can be written as:

$$\delta \left( \int_{\Omega} \mathbf{u}^T \mathbf{b} \, d\Omega + \int_{\Gamma_t} \mathbf{u}^T \mathbf{t} \, d\Gamma - \frac{1}{2} \int_{\Omega} \boldsymbol{\varepsilon}^T \mathbf{C}^E \boldsymbol{\varepsilon} \, d\Omega \right) = 0. \quad (2.18)$$

As it remains being valid for every element in the discretization, Eq. (2.20) can be rewritten in the form:

$$\delta \left( \int_{\Omega^{(e)}} \mathbf{u}^T \mathbf{b} \, d\Omega + \int_{\Gamma_t^{(e)}} \mathbf{u}^T \mathbf{t} \, d\Gamma - \frac{1}{2} \int_{\Omega^{(e)}} \boldsymbol{\varepsilon}^T \mathbf{C}^E \boldsymbol{\varepsilon} \, d\Omega \right) = 0. \quad (2.19)$$

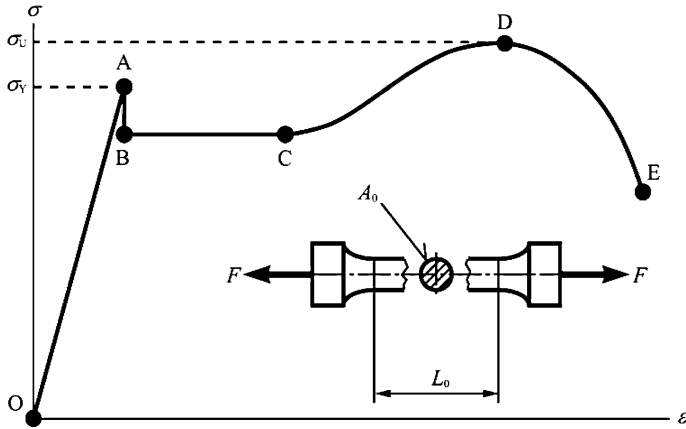


Fig. 2.6 Stress versus strain in a typical tension test

In every element, there are  $N$  points (Fig. 2.6), known as nodes, where the displacements,  $\mathbf{U}^{(e)} = [u_{x1}, u_{y1}, u_{z1}, \dots, u_{xN}, u_{yN}, u_{zN}]^T$ , can be computed and, then, the displacements in other points,  $\mathbf{u}$ , can be interpolated from them:

$$\mathbf{u} = \mathbf{N}\mathbf{U}^{(e)}, \quad (2.20)$$

where  $\mathbf{N}$  is the matrix of shape functions, depending on the coordinates,  $\mathbf{x}$ :

$$\mathbf{N} = \begin{bmatrix} N_1(\mathbf{x}) & 0 & 0 & \dots & N_N(\mathbf{x}) & 0 & 0 \\ 0 & N_1(\mathbf{x}) & 0 & \dots & 0 & N_N(\mathbf{x}) & 0 \\ 0 & 0 & N_1(\mathbf{x}) & \dots & 0 & 0 & N_N(\mathbf{x}) \end{bmatrix}$$

By substituting (2.20) in the weak formulation for an element (2.19), and defining the strain-displacement matrix,  $\mathbf{B} = \nabla_s \mathbf{N}^{(e)}$ , it is obtained the expression:

$$\delta \left( \int_{\Omega^{(e)}} \mathbf{U}^{(e)} \mathbf{N}^{(e)} \mathbf{b} \, d\Omega + \int_{\Gamma_t^{(e)}} \mathbf{U}^{(e)} \mathbf{N}^{(e)} \mathbf{t} \, d\Gamma - \frac{1}{2} \int_{\Omega^{(e)}} \mathbf{U}^{(e)T} \mathbf{B}^T \mathbf{C}^E \mathbf{B} \mathbf{U}^{(e)} \, d\Omega \right) = 0;$$

which is transformed, after applying the rules of variational calculus, in:

$$\int_{\Omega^{(e)}} \mathbf{N}^{(e)} \mathbf{b} \, d\Omega + \int_{\Gamma_t^{(e)}} \mathbf{N}^{(e)} \mathbf{t} \, d\Gamma - \left( \frac{1}{2} \int_{\Omega^{(e)}} \mathbf{B}^T \mathbf{C}^E \mathbf{B} \, d\Omega \right) \mathbf{U}^{(e)} = 0. \quad (2.21)$$

If the stiffness matrix,  $\mathbf{K}^{(e)}$ , and the nodal force vector,  $\mathbf{F}^{(e)}$ , are defined for the element  $e$ , as follows:

$$\mathbf{F}^{(e)} = \int_{\Omega^{(e)}} \mathbf{N}^{(e)} \mathbf{b} \, d\Omega + \int_{\Gamma_t^{(e)}} \mathbf{N}^{(e)} \mathbf{t} \, d\Gamma, \quad (2.22a)$$

$$\mathbf{K}^{(e)} = \left( \frac{1}{2} \int_{\Omega^{(e)}} \mathbf{B}^T \mathbf{C}^E \mathbf{B} \, d\Omega \right); \quad (2.22b)$$

the expression (2.21) can be rewritten as:

$$\mathbf{K}^{(e)}\mathbf{U}^{(e)} = \mathbf{F}^{(e)}. \quad (2.23a)$$

The Eq. (2.23a) for all the elements can be assembled together, by considering the equality of displacement in nodes belonging to different elements, and the action-reaction forces on these nodes, giving a global equation involving all the nodal displacement,  $\mathbf{U}$ , and forces,  $\mathbf{F}$ :

$$\mathbf{KU} = \mathbf{F} \quad (2.23b)$$

which is an algebraic equation set of the form (2.6).

By considering the essential boundary conditions at nodes belonging to  $\Gamma_u$ , and natural boundary conditions nodes belonging to  $\Gamma_t$ , the system (2.23b) can be simplified, usually by deleting rows and columns corresponding to null degrees of freedom. Then, the obtained system:

$$\tilde{\mathbf{K}}\tilde{\mathbf{U}} = \tilde{\mathbf{F}}; \quad (2.24a)$$

can be numerically solved in order to determine the nodal displacements:

$$\tilde{\mathbf{U}} = \tilde{\mathbf{K}}^{-1}\tilde{\mathbf{F}}. \quad (2.24b)$$

## 2.3 FEM for Plasticity

### 2.3.1 Plasticity Fundamentals

As the most important manufacturing processes, such as machining and forming, involves plastic deformations, modeling the plasticity and solving the obtaining models by using numeric methods play a key role in simulation of these processes.

Plasticity can be broadly classified in two types: rate-independent plasticity, where the strain rate has no influence in the strain–stress relationship, and viscoplasticity, where the strain rate has a non-negligible influence. The first one is a good approximation when low strain rates take place in the deformation process; on the contrary, when the strain rates are high, viscoplasticity offers better results.

The behavior of the materials in rate-independent plasticity can be studied through a standard tension test (see Fig. 2.6), where the values of the true stress,  $\sigma$ :

$$\sigma = \sigma_0(1 + \varepsilon); \quad (2.25)$$

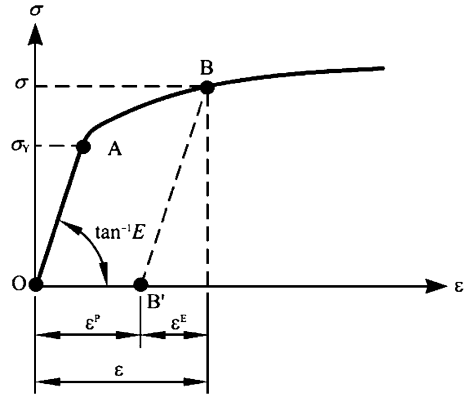
are plotted versus the logarithmic strain,  $\varepsilon$ :

$$\varepsilon = \ln(1 + e); \quad (2.26)$$

where  $\sigma_0 = F/A_0$  is the engineering stress applied in the test and  $e = (L-L_0)/L_0$  is the infinitesimal linear strain.



**Fig. 2.7** Elastic and plastic components of the strain



In Fig. 2.6 it is represented a typical experimental stress–strain curve, corresponding to a mild steel (Han and Reddy 1999). Some different regions can be identified in this curve. In portion OA, there is a linear proportionality between the strain and stress (which is given by the Young’s modulus,  $E$ ), and when the load is retired, the material return to the unloaded initial condition (point O). This kind of deformation is known as linear elastic, and follows the previously mentioned Hooke’s law (2.6).

When the stress surpasses some value (called yield stress,  $\sigma_Y$ ), there is a sharp sudden drop in the stress value (region AB). The region BC is characterized for a near zero slope in the curve, that is to say that increments in the strain take place without any rise in the stress value. The region CD is known as the hardening region, because the stress increases with the strain, although not with linear relationship, until achieving the ultimate strength,  $\sigma_U$ , at point D. On the contrary, in region DE (softening region) increments in strain cause a decrease in the stress until the final failure at point E.

Even though this curve is representative, actual behavior can strongly change from one material to another one. Even, heat treatments can change the form of this curve for the same material.

In spite of the complexity of the material behavior, two well defined zones can be identified: an elastic region, where deformations disappear after removing the load, and a plastic region, where some deformations stay after removing the load (see Fig. 2.7). Therefore, every strain,  $\varepsilon$ , at the plastic zone can be considered as composed by an elastic strain,  $\varepsilon^E$ , and a plastic strain,  $\varepsilon^P$ :

$$\varepsilon = \varepsilon^E + \varepsilon^P. \quad (2.27)$$

### 2.3.2 Material Behavior Models

Due to the complexity of the experimental plastic behavior of engineering materials it has been idealized by using simpler models (see Fig. 2.8).

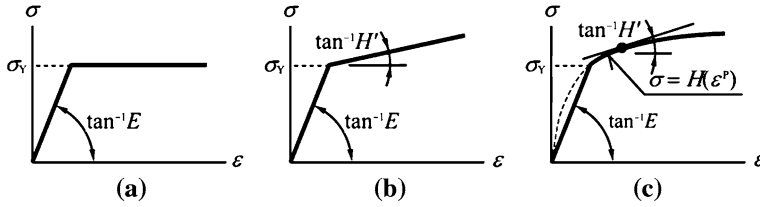


**Fig. 2.8** Idealized plastic behavior of materials **a** Elastic-perfectly plastic. **b** Linear work-hardening. **c** Nonlinear work-hardening

In the elastic-perfectly plastic idealization (Fig. 2.8a), there is not further increment in the stress after surpassing the yield point. On the contrary, in the elastic-work-hardening idealization (Fig. 2.8b, c), the stress continues rising with strain increments after the yield point. This increment is modeled by the material hardening function,  $H$ :

$$\sigma = H(\varepsilon^P). \quad (2.28)$$

For linear work-hardening (Fig. 2.8b), the plastic behavior is represented by a straight line with a constant slope  $H'$ , while in the nonlinear work-hardening (Fig. 2.8c), the curve changes its slope  $H' = dH/d\varepsilon^P$ .

Several models have been proposed for the material hardening deformation. The simplest consider that stress is only a function of the strain and not of the strain rate. They are called strain rate-independent plastic models, and include, among others, (Dixit et al. 2011), the Hollomon's law:

$$\sigma = K(\varepsilon^P)^n; \quad (2.29a)$$

that does not fit the stress–strain relationship at low strains; the Ludwik's law:

$$\sigma = \sigma_Y + K(\varepsilon^P)^n; \quad (2.29b)$$

that does not reflect properly the constant slope of the stress–strain curve of metals at large strain; the Swift's law:

$$\sigma = \sigma_Y(1 + K\varepsilon^P)^n; \quad (2.29c)$$

which fits better the behavior of the stress–strain curve of metal at large strain; and the Voce's law:

$$\sigma = \sigma_Y + K[1 - m \exp(-n\varepsilon^P)]; \quad (2.29d)$$

that is more suitable for moderate strain values. In all of these expressions,  $K$  and  $n$  are experimental constants describing the plastic behavior of the material.

In some circumstances, the effect of the strain-rate cannot be neglected, for example, in cutting processes where high values of strain rates take place. This cases, which include the plastic strain rate term,  $\dot{\varepsilon}^P$ , in the material hardening

function are known as viscoplastic models. If the expression also includes the temperature,  $T$ , then it is called thermo-viscoplastic model.

Determination of viscoplastic and thermo-viscoplastic models cannot be carried out through single tension test. It requires more complex methods such as the split Hopkinson pressure bar (Jasper and Dautzenberg 2002). An example of thermo-viscoplastic model is the generalized Oxley's equation (Lalwani et al. 2009):

$$\sigma = \sigma_1(T_{\text{mod}})(\dot{\varepsilon}^{\text{P}})^{n(T_{\text{mod}})}; \quad (2.30a)$$

where the coefficient  $\sigma_1$  and the exponent  $n$  are polynomial functions of the strain-modified temperature,  $T_{\text{mod}}$ :

$$T_{\text{mod}} = T \left( 1 - v \log_{10} \frac{\dot{\varepsilon}^{\text{P}}}{\dot{\varepsilon}_0^{\text{P}}} \right); \quad (2.30b)$$

which depends on the material temperature,  $T$ , the plastic strain rate,  $\dot{\varepsilon}^{\text{P}}$ , the reference plastic strain rate,  $\dot{\varepsilon}_0^{\text{P}}$ , and the strain rate sensitivity constant,  $v$ .

The Johnson–Cook's model, also referred as J–C law, is other of the frequently used empirical approaches for modeling the thermo-viscoplastic behavior of materials. It is described by the expression (Özel and Zeren 2004):

$$\sigma = [A + B(\varepsilon^{\text{P}})^n] \left[ 1 + C \ln \left( \frac{\dot{\varepsilon}^{\text{P}}}{\dot{\varepsilon}_0^{\text{P}}} \right) \right] \left[ 1 - \left( \frac{T - T_0}{T_{\text{M}} - T_0} \right)^m \right]; \quad (2.30c)$$

where the  $\varepsilon$  is the plastic strain,  $\dot{\varepsilon}^{\text{P}}$  is the plastic strain rate,  $\dot{\varepsilon}_0$  is the reference strain rate,  $T$  is the absolute temperature of the material,  $T_{\text{M}}$  is the melting temperature,  $T_0$  is the reference temperature and  $A$ ,  $B$ ,  $C$ ,  $n$  and  $m$  are material constants ( $A$  is the yield strength at  $T_0$ ,  $B$  is the hardening modulus,  $C$  is the strain rate sensitivity,  $n$  is the strain-hardening exponent, and  $m$  the thermal softening exponent). In spite of some limitations with regard to dynamics train aging, i.e. blue-brittleness effect during a certain range of temperature variations in the plastic deformation of carbon steels, the J–C law is very often used to represent the thermo-viscoplastic behavior of workpiece material in manufacturing process modeling, especially in cutting processes (Arrazola and Özel 2010).

Sometimes, the so-called power law (Dixit et al. 2011) is also used for describing the behavior of materials at thermo-viscoplastic state:

$$\sigma = \sigma_0(\dot{\varepsilon}^{\text{P}})^n \left( \frac{\dot{\varepsilon}^{\text{P}}}{\dot{\varepsilon}_0^{\text{P}}} \right)^m \left( \frac{T}{T_0} \right)^{-r}; \quad (2.30d)$$

where the terms has the same meaning than in the previous expressions. As in the J–C model, in the power law the effects of strain, strain rate and temperature are considered independent.

Applying the dislocation mechanics theory, Zerilli and Armstrong (Jasper and Dautzenberg 2002) derived other more complex constitutive models for body-centered cubic metals:

$$\sigma = C_0 + C_1 \exp\left(-C_3 T + C_4 T \ln \frac{\dot{\varepsilon}}{\dot{\varepsilon}_0}\right) + C_5 \varepsilon^n; \quad (2.30e)$$

and for face-centered cubic metal:

$$\sigma = C_0 + C_2 \varepsilon^{1/2} \exp\left(-C_3 T + C_4 T \ln \frac{\dot{\varepsilon}}{\dot{\varepsilon}_0}\right); \quad (2.30f)$$

where  $C_0, C_1, \dots, C_5$  are material properties. These models has the advantage of a strong theoretical component, however, they have not been as widely applied in FEM-based modeling of manufacturing process as J-C model or Oxley's equation.

### 2.3.3 Yielding Criteria

Another important aspect, in the theory of plasticity is the initial yielding criterion, that is, the point at which the yield process starts, As follows from Fig. 2.6, the criterion for initial yielding in simple tension is given by:

$$\sigma - \sigma_Y = 0; \quad (2.31)$$

where  $\sigma$  is the tensile stress and  $\sigma_Y$ , the yield stress of the material. However, more complex stress states require more elaborated criteria. One of the most used criteria for defining the beginning of the yielding process in a material is the Von Mises' criterion, which established that the yield begins when resultant deviatoric stress reaches a critical value. In terms of the principal stresses,  $\sigma_1, \sigma_2$  and  $\sigma_3$ , this can be written as:

$$[(\sigma_1 - \sigma_2)^2 + (\sigma_2 - \sigma_3)^2 + (\sigma_3 - \sigma_1)^2] - 2\sigma_Y^2 = 0. \quad (2.32)$$

On the other hand, the so-called Tresca's criterion, defines the initial yielding from the maximum shear stress, and can be expressed by the equation:

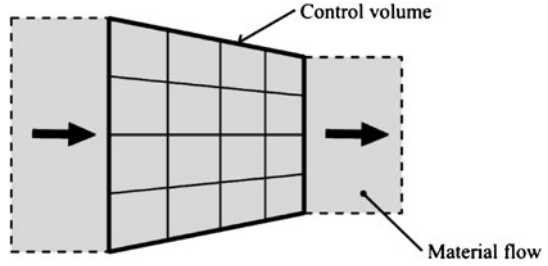
$$[(\sigma_1 - \sigma_2)^2 - \sigma_Y^2][(\sigma_2 - \sigma_3)^2 - \sigma_Y^2][(\sigma_3 - \sigma_1)^2 - \sigma_Y^2] = 0. \quad (2.33)$$

### 2.3.4 Governing Equations

Contrary to what happens in elasticity, in plasticity the stress depends on the history of deformation. Mathematically, this can be expressed by using either the incremental form or the rate form (Shabana 2008).

The rate form is used in the so-called Eulerian formulation of the continuum, which considers that the reference coordinate system is fixed and the material moves through it (Fig. 2.9). This approach is very convenient when the material flows through a fixed region of the space, known as control volume, which is used

**Fig. 2.9** Eulerian formulation of the continuum



as the problem domain. This Eulerian formulation is frequently applied in extrusion, rolling and other cold forming processes. It is also used in metal cutting, if the shape of the chip is previously known.

There are three main governing equation sets in the Eulerian formulation (Dixit and Dixit 2008). The first one is the kinematic relationship between the velocity vector,  $v_i$ , and the strain rate tensor,  $\dot{\epsilon}_{ij}$ , which provides six scalar equations<sup>1</sup>:

$$\dot{\epsilon}_{ij} = \frac{1}{2} \left( \frac{\partial v_i}{\partial x_j} + \frac{\partial v_j}{\partial x_i} \right). \quad (2.34)$$

and the velocity is defined as the rate of change of the material position,  $x_i$ :

$$v_i = \frac{dx_i}{dt}. \quad (2.35)$$

The constitutive relation links the elastic-plastic stress and the strain rate and provides other six scalar equations:

$$\dot{\epsilon}_{kk} = \frac{\dot{s}_{kk}}{3K}; \quad (2.36a)$$

$$\dot{\epsilon}'_{ij} = \frac{1}{2G} \dot{s}'_{kk} + \frac{3\dot{\epsilon}_{eq}^P}{2\sigma_{eq}} \sigma'_{ij}; \quad (2.36b)$$

where  $G$  and  $K$  are the shear modulus and the bulk modulus of the material;  $\dot{\epsilon}'_{ij}$  is the deviatoric part of the strain rate tensor:

$$\dot{\epsilon}'_{ij} = \dot{\epsilon}_{ij} - \frac{1}{3} \delta_{ij} \dot{\epsilon}_{kk}; \quad (2.37)$$

$\delta_{ij}$  is the Kronecker delta;  $\sigma_{eq}$  is the Von Mises equivalent stress:

$$\sigma_{eq} = \sqrt{\frac{3}{2} \sigma'_{ij} \sigma'_{ij}}; \quad (2.38)$$

<sup>1</sup> For an explanation of the index notation and summation convention used in this section, see Dixit and Dixit (2008, §2.2) or Shabana (2008, §1.3).

$\sigma'_{ij}$  is the deviatoric part of the stress tensor:

$$\sigma'_{ij} = \sigma_{ij} - \frac{1}{3} \delta_{ij} \sigma_{kk}; \quad (2.39)$$

$\dot{\epsilon}_{eq}^P$  is the equivalent plastic strain tensor:

$$\dot{\epsilon}_{eq}^P = \sqrt{\frac{2}{3} \dot{\epsilon}_{ij}^P \dot{\epsilon}_{ij}^P}; \quad (2.40)$$

$\dot{s}_{ij}$  is the Jaumann stress rate tensor, which is related with the Cauchy stress rate tensor,  $\dot{\sigma}_{ij}$ , by the expressions:

$$\dot{s}_{kk} = \dot{\sigma}_{kk} - (\dot{\omega}_{kl} \sigma_{lk} + \sigma_{kl} \dot{\omega}_{lk}^T); \quad (2.41a)$$

$$\dot{s}'_{ij} = \dot{\sigma}'_{ij} - (\dot{\omega}_{il} \sigma'_{lj} + \sigma'_{il} \dot{\omega}_{lj}^T); \quad (2.41b)$$

and  $\dot{\omega}_{ij}$  is the spin tensor:

$$\dot{\omega}_{ij} = \frac{1}{2} \left( \frac{\partial v_i}{\partial x_j} - \frac{\partial v_j}{\partial x_i} \right). \quad (2.42)$$

The value of the equivalent stress is related with the equivalent strain by the material hardening function:

$$\sigma_{eq} = H(\epsilon_{eq}^P); \quad (2.43a)$$

which can also include the strain rate and temperature term, in the general case of thermo-viscoplastic behavior:

$$\sigma_{eq} = H(\epsilon_{eq}^P, \dot{\epsilon}_{eq}^P, T). \quad (2.43b)$$

The third set is given by the motion equation, which consist on three scalar equations:

$$\rho \left( \frac{\partial x_i}{\partial t} + \frac{\partial v_i}{\partial x_j} v_j \right) = \rho b_i + \frac{\partial \sigma_{ij}}{\partial x_j}; \quad (2.44)$$

where  $\rho$  is the material density and  $b_i$  the body force vector.

Additionally, the boundary conditions must be considered. On one hand, the velocity components,  $[v]_i$ , must be known at some sections of the boundary,  $\Gamma_v$ :

$$v_i = [v]_i, \quad \text{on } \Gamma_v. \quad (2.45a)$$

On the other hand, the values of tension vector,  $[t^n]_i$ , along the normal to the surface,  $n_i$ , must be prescribed on some part of the boundary,  $\Gamma_t$ :

$$\sigma_{ij} n_j = [t^n]_i, \quad \text{on } \Gamma_t. \quad (2.45b)$$

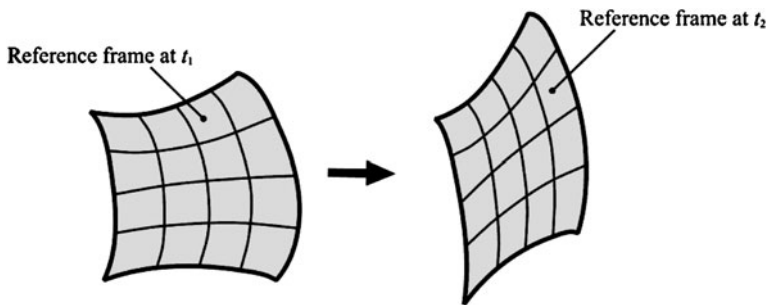


**Fig. 2.10** Lagrangian formulation of the continuum

Finally, when dealing with a transient problem, the initial values of the velocities, and hydrostatic and deviatoric part of the stress must be known at every point of the domain,  $\Omega$ :

$$v_i = v_i^0, \quad \sigma_{kk} = \sigma_{kk}^0, \quad \sigma'_{ij} = \sigma'_{ij}{}^0, \quad \text{at } t = t_0, \quad \forall x_i \in \Omega. \quad (2.46)$$

In steady-state problems, these initial conditions are not need.

If the behavior of the material is considered as rigid-plastic (i.e., the elastic part of the strain is neglected), an interesting simplification takes place. In this case, the constitutive relation take the form:

$$\dot{\epsilon}_{kk} = 0; \quad (2.47a)$$

$$\dot{\epsilon}'_{ij} = \frac{3\dot{\epsilon}_{eq}^P}{2\sigma_{eq}} \sigma'_{ij}; \quad (2.47b)$$

This change is not trivial because the time derivative of the stress tensor disappears from the constitutive relations (2.47a, b). Thence, although still being nonlinear and, therefore, requiring an iterative solving scheme, the solution of the problem is easier than in the elastic-plastic formulation. Furthermore, only the velocities at the start time are needed as initial conditions.

Nevertheless, the rigid-plastic formulation has some shortcomings related with the neglect of the elastic component of the strain. For example, neither the stress distribution in the non-plastic region nor the residual stresses can be computed by using this approach.

The Lagrangian formulation uses a reference frame which is attached to the material and moves together with it (Fig. 2.10). It is very convenient when the space occupied by the material is not previously known as in free forging or transient cutting analysis.

The Lagrangian approach uses the incremental form which is based on the use of the incremental strain tensor,  $d\epsilon_{ij}$  (Dixit and Dixit 2008):

$$d\epsilon_{ij} = \frac{1}{2} \left[ \frac{\partial(du_i)}{\partial x_j} + \frac{\partial(du_j)}{\partial x_i} \right]; \quad (2.48)$$

defined from the incremental displacement vector,  $du_i$ :

$$du_i = x_i(t + dt) - x_i(t); \quad (2.49)$$

where  $x_i(t)$  is the position of a particle at instant  $t$ , and  $dt$  is the differential increment of time.

In the incremental strain tensor, the component  $d\epsilon_{ii}$  represents the change in current length per unit of current length along the current  $i$ -axis direction. The component  $d\epsilon_{ij}$  represents half the change in angle between the current  $i$ - and  $j$ -axes directions.

Both, the incremental strain tensor and the strain rate tensor are related by:

$$d\epsilon = \dot{\epsilon} dt. \quad (2.50)$$

The constitutive relation links the incremental strain tensor with the increment Jaumann stress tensor,  $ds_{ij}$ , or the stress rate tensor. After yielding, i.e., for the elastic–plastic behavior, this constitutive relation can be expressed as:

$$ds_{ij} = C_{ijkl}^{EP} d\epsilon_{kl}; \quad (2.51)$$

where  $C_{ijkl}^{EP}$  is the fourth order elasticity–plasticity tensor:

$$C_{ijkl}^{EP} = 2G \left[ \frac{\nu}{1 - 2\nu} \delta_{ij} \delta_{kl} + \delta_{ik} \delta_{jl} - \frac{9G}{2} \frac{\sigma'_{ij} \sigma'_{ij}}{(H' + 3G) \sigma_{eq}^2} \right]; \quad (2.52)$$

$G$  is the shear modulus;  $\nu$  is the Poisson's ratio; and  $H'$ , is the slope of the hardening function of the material (Eq. 2.41a, b);  $\sigma_{eq}$  is the equivalent stress (Eq. 2.38), and is  $\sigma'_{ij}$ , the deviatoric part of the stress tensor (Eq. 2.39).

Before yielding and after unloading, i.e., when material is behaving elastically, the constitutive equation takes the form:

$$ds_{ij} = C_{ijkl}^E d\epsilon_{kl}; \quad (2.53)$$

being:

$$C_{ijkl}^E = 2G \left( \frac{\nu}{1 - 2\nu} \delta_{ij} \delta_{kl} + \delta_{ik} \delta_{jl} \right). \quad (2.54)$$

The incremental Jaumann stress tensor is related with the incremental Cauchy stress tensor by the equation:

$$ds_{ij} = s_{ij} dt = d\sigma_{ij} - (d\omega_{il} \sigma_{lj} + \sigma_{il} d\omega_{lj}^T); \quad (2.55)$$

where the incremental infinitesimal rotation tensor,  $d\omega_{ij}$ , is defined as:

$$d\omega_{ij} = \frac{1}{2} \left[ d \left( \frac{\partial u_i}{\partial x_j} \right) - d \left( \frac{\partial u_j}{\partial x_i} \right) \right]. \quad (2.56)$$



The incremental equation of motion states that:

$$\rho da_i = \rho db_i + d\left(\frac{\partial \sigma_{ij}}{\partial x_j}\right); \quad (2.57)$$

where  $db_i$  is the incremental body force and  $da_i$  is the incremental acceleration.

For the Lagrangian formulation, the required boundary conditions are defined by the prescribed incremental displacements,  $[du]_i$ , at some region  $\Gamma_u$ :

$$du_i = [du]_i, \quad \text{on } \Gamma_u \quad (2.58a)$$

and the prescribed tension vectors  $[t^n]_i$  along the normal,  $n_i$ , on some region  $\Gamma_t$ :

$$d\sigma_{ij}n_j = [dt^n]_i, \quad \text{on } \Gamma_u. \quad (2.58b)$$

The initial conditions include values of the incremental displacements,  $du_i$ , and incremental velocities,  $dv_i$ , at time  $t_0$ , in every point of the problem domain,  $\Omega$ :

$$du_i = du_i^0, \quad dv_i = dv_i^0, \quad \text{at } t = t_0, \quad \forall x_i \in \Omega. \quad (2.59)$$

### 2.3.5 FEM Formulation

In the Eulerian finite element formulation, for elastic–plasticity is based in the equation:

$$\mathbf{K}^{(e)} \mathbf{V}^{(e)} = \dot{\mathbf{F}}^{(e)}; \quad (2.60)$$

where  $\mathbf{V}^{(e)} = [v_{x1}, v_{y1}, v_{z1}, \dots, v_{xN}, v_{yN}, v_{zN}]^T$  is the vector of nodal velocities;  $\dot{\mathbf{F}}^{(e)} = [\dot{f}_{x1}, \dot{f}_{y1}, \dot{f}_{z1}, \dots, \dot{f}_{xN}, \dot{f}_{yN}, \dot{f}_{zN}]^T$  is the vector of nodal forces;  $\mathbf{K}^{(e)}$  is the element stiffness matrix, given by:

$$\mathbf{K}^{(e)} = \frac{1}{2} \int_{\Omega^{(e)}} \mathbf{B}^T \mathbf{C}^{\text{EP}} \mathbf{B} d\Omega; \quad (2.61)$$

and  $\mathbf{C}^{\text{EP}}$  is the elastic–plastic matrix:

$$\mathbf{C}^{\text{EP}} = \mathbf{C}^{\text{E}} - \frac{9G^2}{(H' + 3G)\sigma_{\text{eq}}^2} \begin{bmatrix} \sigma'_{xx} \sigma'_{xx} & \sigma'_{yy} \sigma'_{xx} & \sigma'_{zz} \sigma'_{xx} & 2\sigma'_{xy} \sigma'_{xx} & 2\sigma'_{yz} \sigma'_{xx} & 2\sigma'_{zx} \sigma'_{xx} \\ \sigma'_{xx} \sigma'_{yy} & \sigma'_{yy} \sigma'_{yy} & \sigma'_{zz} \sigma'_{yy} & 2\sigma'_{xy} \sigma'_{yy} & 2\sigma'_{yz} \sigma'_{yy} & 2\sigma'_{zx} \sigma'_{yy} \\ \sigma'_{xx} \sigma'_{zz} & \sigma'_{yy} \sigma'_{zz} & \sigma'_{zz} \sigma'_{zz} & 2\sigma'_{xy} \sigma'_{zz} & 2\sigma'_{yz} \sigma'_{zz} & 2\sigma'_{zx} \sigma'_{zz} \\ \sigma'_{xx} \sigma'_{xy} & \sigma'_{yy} \sigma'_{xy} & \sigma'_{zz} \sigma'_{xy} & 2\sigma'_{xy} \sigma'_{xy} & 2\sigma'_{yz} \sigma'_{xy} & 2\sigma'_{zx} \sigma'_{xy} \\ \sigma'_{xx} \sigma'_{yz} & \sigma'_{yy} \sigma'_{yz} & \sigma'_{zz} \sigma'_{yz} & 2\sigma'_{xy} \sigma'_{yz} & 2\sigma'_{yz} \sigma'_{yz} & 2\sigma'_{zx} \sigma'_{yz} \\ \sigma'_{xx} \sigma'_{zx} & \sigma'_{yy} \sigma'_{zx} & \sigma'_{zz} \sigma'_{zx} & 2\sigma'_{xy} \sigma'_{zx} & 2\sigma'_{yz} \sigma'_{zx} & 2\sigma'_{zx} \sigma'_{zx} \end{bmatrix}. \quad (2.62)$$

In the former equation,  $\mathbf{C}^E$  represents the elasticity matrix (Eq. 2.13b),  $G$  is the shear modulus;  $H'$  is the slope of the material hardening function; and  $\sigma_{eq}$  is the equivalent stress, determined from the hardening function (Eq. 2.43a, b).

The Lagrangian finite element formulation is based on the equation:

$$\mathbf{K}^{(e)} d\mathbf{U}^{(e)} = d\mathbf{F}^{(e)}; \quad (2.63)$$

where  $d\mathbf{U}^{(e)} = [du_{x1}, du_{y1}, du_{z1}, \dots, du_{xN}, du_{yN}, du_{zN}]^T$  is the vector of incremental nodal displacements; and  $d\mathbf{F}^{(e)} = [df_{x1}, df_{y1}, df_{z1}, \dots, df_{xN}, df_{yN}, df_{zN}]^T$  is the vector of incremental nodal forces.  $\mathbf{K}^{(e)}$  is the element stiffness matrix, given by (2.61).

As the stiffness matrix involves the components of the deviatoric part of the stress tensor, equations (2.60) and (2.63) are nonlinear and cannot be solved straightforwardly but numerically integrated. This integration is usually performed by a generalized midpoint rule (Wriggers 2008):

$$u_{n+1} = u_n + \Delta t f(u_{n+\theta}); \quad (2.64a)$$

$$u_{n+\theta} = (1 - \theta)u_n + \theta u_{n+1}, \quad 0 \leq \theta \leq 1. \quad (2.64b)$$

For  $\theta = 0$ , this equations lead to the explicit Euler scheme; for  $\theta = 1$ , they lead to the implicit Euler scheme; finally, for  $\theta = 1/2$ , they lead to the midpoint rule.

There is, also, a mixed approach, known as arbitrary Lagrangian–Eulerian (ALE) formulation, which has been widely used in recent years especially in modeling of cutting processes. It combines the features of pure Lagrangian analysis in which the mesh follows the material and Eulerian analysis where the mesh is fixed, when is needed as part of the adaptive remeshing.

In an ALE approach the process starts with an initial formed chip geometry, which is iteratively modified as the analysis proceeds until converging to the final shape of the chip (Vaziri et al. 2011).

Other approach in the ALE formulation allows the simulation of the chip formation, starting from zero, through a transient analysis. This method requires kinematic penalty contact conditions between the tool and the workpiece (Arrazola and Özel 2010).

A more detailed explanation on the ALE formulation, including the used algorithms and equations can be found in (Pantalé et al. 2004 and Olovsson et al. 1999).

## 2.4 Thermal Analysis

Thermal phenomena must be taken into account in FEM-based modeling of manufacturing processes, especially in machining and hot forming. Not only in the chip, but also in the tool, temperature,  $T$ , behavior is governed by the so-called Fourier's law (Li et al. 2002):

$$\kappa \nabla^2 T - \rho c \dot{T} + \dot{Q} = 0; \quad (2.65)$$

where  $\nabla^2$  is the Laplace's operator;  $\kappa$  and  $c$  are the thermal conductivity and specific heat of the material; and  $\dot{Q}$  is the rate of generated heat.

There are two main sources of heat generation in processes involving metal working: plastic deformation and friction. The heat generated by plastic deformation can be computed by:

$$\dot{Q}_p = \eta_p \boldsymbol{\sigma} : \dot{\boldsymbol{\epsilon}}^p; \quad (2.66)$$

being  $\eta_p$  the fraction of plastic work transformed into heat (usually  $\eta_p \approx 0.9$ );  $\boldsymbol{\sigma}$  the Cauchy stress tensor and  $\dot{\boldsymbol{\epsilon}}^p$  the plastic strain tensor.

The heat generated by friction is given by:

$$\dot{Q}_f = \eta_f \tau_f v_s; \quad (2.67)$$

where  $\eta_f$  is the fraction of friction work transformed into heat (for machining applications  $\eta_f \approx 1$ ),  $\tau_f$  is the friction shear stress and  $v_s$  is the sliding velocity.

The heat flux,  $q$ , to the environment, from the free surfaces of the tool and part can be computed by the Newton's law of cooling (Grzesik 2006):

$$q = h(T_w - T_0); \quad (2.68)$$

where  $h$  is the convection heat transfer,  $T_w$  is the wall temperature and  $T_0$  is the room temperature.

For computational efficiency, temperature discretization and computation are carried out together with the solution of the plasticity problem, in the so-called coupled formulation.

## 2.5 Friction Models

Friction is very important factor in most of the machining processes. Friction between the tool and chip, in cutting processes, has a strong influence on the forces and temperature and, consequently, on the operation economy. In forming processes, friction also plays a crucial role.

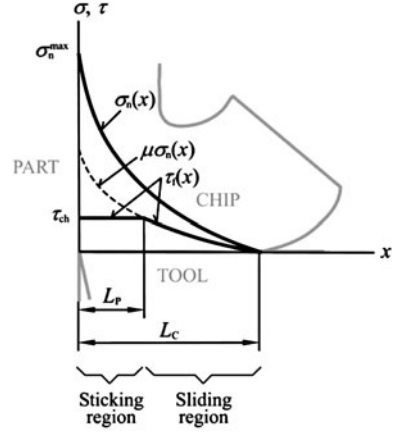
The simplest friction law is the so-called Coulomb's law, which considers a constant friction factor,  $\mu$ , relating the friction shear stress,  $\tau_f$ , and the normal stress acting on the surface,  $\sigma_n$ :

$$\tau_f = \mu \sigma_n. \quad (2.69)$$

Although in concordance with empirical data, this expression fails matching the friction behavior at high pressures and sliding velocities, such as those taking place in cutting processes. Therefore, other more complex models have been proposed.

Coulomb's law sometimes contains a term,  $b$ , representing the cohesion sliding resistance (i.e., sliding resistance with zero normal pressure) (Pramanik et al. 2007):

**Fig. 2.11** Stress distribution at the tool rake face



$$\tau_f = \mu\sigma_n + b; \quad (2.70)$$

although this parameter is usually neglected in machining simulations.

A modified Coulomb's law, proposed by Zorev (Vaziri et al. 2011) considers two different regions from the friction point of view. In the sliding region, where elastic contact exists, the value of the friction shear stress is proportional to the normal stress. In the sticking region, where plastic friction takes place, it is constant and equal to the average shear flow stress of the chip material on the chip-tool interface,  $\tau_{ch}$ :

$$\tau_f = \begin{cases} \mu\sigma_n & : \mu\sigma_n < \tau_{ch} \quad (0 \leq x \leq L_p) \quad (\text{sliding region}) \\ \tau_{ch} & : \mu\sigma_n \geq \tau_{ch} \quad (L_p < x \leq L_c) \quad (\text{sticking region}) \end{cases}. \quad (2.71)$$

The average shear flow stress in the sticking region can be considered as equal to the material yield shear stress,  $\tau_Y$  (Zhang et al. 2011):

$$\tau_{ch} = \tau_Y = \frac{\sigma_Y}{\sqrt{3}}. \quad (2.72)$$

The distribution of the normal stress through the rake face (Fig. 2.11) can be approximately modeled by the following empirical relationship (Mohammadpour et al. 2010):

$$\sigma_n = \sigma_n^{\max} \left[ 1 - \left( \frac{x}{L_c} \right)^a \right]; \quad (2.73)$$

where  $L_c$  is the chip-tool contact length,  $\sigma_n^{\max}$  is the maximum normal stress and  $a$  is an empirical constant.

The Usui and Shirakashi's model (Filice et al. 2007) relates the friction shear stress with the normal stress and the flow shear stress by using a more complex expression:

$$\tau_f = \tau_{ch} \left[ 1 - \exp \left( -\frac{\mu \sigma_n}{\tau_{ch}} \right) \right]. \quad (2.74a)$$

which has been modified by Childs and coworkers by adding a proportionality term,  $m$  ( $0 < m < 1$ ) (Filice et al. 2007):

$$\tau_f = m \tau_{ch} \left[ 1 - \exp \left( -\frac{\mu \sigma_n}{\tau_{ch}} \right) \right]. \quad (2.74b)$$

Other interesting approach is the cohesive model (Mamalis et al. 2002), which constitutes an idealized model of the influence of the elastic-plastic deformation of the asperities at the metal surface at microscopic scale (cold weld phenomenon). This model establishes that:

$$\tau_f = -m \frac{2\sigma_{eq}}{3\sqrt{3}} \tan^{-1} \left( \frac{v_s}{c} \right); \quad (2.75)$$

where  $m$  is the shear friction factor;  $\sigma_{eq}$  is the equivalent stress,  $v_s$  is the sliding velocity and  $c$  is a constant representing the value of sliding velocity at which sliding occurs.

Sometimes, it results more convenient to obtain empirical expressions relation the friction factor with other parameters. For example, Rech et al. (2009) divide the apparent friction factor,  $\mu_{app}$ , into a component due to the plastic deformation,  $\mu_{plast}$ , and another one due to adhesive phenomena,  $\mu_{adh}$ :

$$\mu_{app} = \mu_{plast} + \mu_{adh}; \quad (2.76)$$

having the adhesive component a linear dependency with the average local sliding velocity for a combination of annealed AISI 1045 steel and TiN-coated carbide.

Also for AISI 1045 steel and uncoated carbide, Brocail et al. (2010) have obtained, through FEM simulation, the exponential model:

$$\mu = 0.919 \sigma_n^{-0.251} v_s^{-0.0463} T_{int}^{0.480}; \quad (2.77)$$

relating the friction factor,  $\mu$ , with the normal stress,  $\sigma_n$ , the sliding velocity,  $v_s$ , and the temperature at the interface,  $T_{int}$ .

In spite of the success of these models in some cases, more experimental and theoretical research is required in this field, in order to obtain actually reliable and flexible friction models.

## 2.6 Fracture

In Lagrangian and ALE formulation there is a need of use some fracture criterion which allows evaluating the state of damage of the elements and carries out the separation of the chip in cutting processes and the breakage of the workpiece in forming.

Nearly all the strain–stress based fracture criteria came from the Freudenthal’s criterion, which considers that fracture takes place when the plastic work per unit volume reaches some critical value,  $C_1$  (Gouveia et al. 2000):

$$\int_0^{\varepsilon_{eq}^F} \sigma_{eq} d\varepsilon_{eq} = C_1; \quad (2.78)$$

where  $\sigma_{eq}$  and  $\varepsilon_{eq}$  are the equivalent stress and strain, respectively, and  $\varepsilon_{eq}^F$  is the value of equivalent strain at which the fracture take place.

The normalized Cockcroft-Latham criterion uses the relation between the largest principal stress,  $\sigma_1$ , and the equivalent stress,  $\sigma_{eq}$  (Umbrello 2008):

$$\int_0^{\varepsilon_{eq}^F} \frac{\sigma_1}{\sigma_{eq}} d\varepsilon_{eq} = C_2; \quad (2.79)$$

while the Brozzo’s equation combines the effects of the principal stress,  $\sigma_1$ , and the hydrostatic stress,  $p$  (Gouveia et al. 2000):

$$\int_0^{\varepsilon_{eq}^F} \frac{2\sigma_1}{3(\sigma_1 - p)} d\varepsilon_{eq} = C_3. \quad (2.80)$$

Another approach (Rosa et al. 2007), which is based on the specific distortion energy, states that the ductile damage takes place when:

$$\int_0^{\gamma^F} \tau d\gamma = C_4; \quad (2.81)$$

where  $\tau$  and  $\gamma$  are the shear stress and the distortion of the element, and  $\gamma^F$  is the level of material distortion at the onset of cracking.

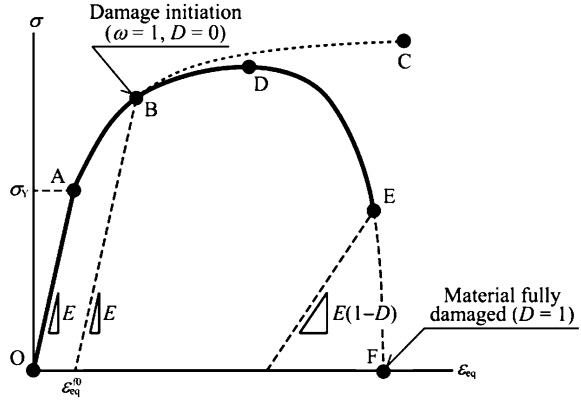
The stress index parameter is also used as a fracture criterion (Shet and Deng 2003). It is defined as:

$$f = \sqrt{\left(\frac{\sigma_n}{\sigma_F}\right)^2 + \left(\frac{\tau}{\tau_F}\right)^2}; \quad (2.82a)$$

where  $\sigma_F$  and  $\tau_F$  are the failure stresses of the material under pure tensile and shear loading conditions. The fracture starts when the stress index parameter reaches the value of one:

$$f \geq 1. \quad (2.83b)$$

**Fig. 2.12** Typical stress–strain material response with damage



A more elaborated damage approach is the Johnson–Cook’s shear failure model (Zhang et al. 2011) with damage starting at point B (see Fig. 2.12), where the cumulative scalar parameter:

$$\omega = \sum_{j=1}^n \left( \frac{\Delta \epsilon_{eq}^P}{\epsilon_{eq}^{f0}} \right)_j; \quad (2.84)$$

exceeds 1. In Eq. (2.84)  $\Delta \epsilon_{eq}^P$  is the increment of equivalent plastic strain in the computation step  $j$ , and:

$$\epsilon_{eq}^{f0} = \left[ d_1 + d_2 \exp \left( d_3 \frac{p}{\sigma_{eq}} \right) \right] \left[ 1 + d_4 \ln \left( \frac{\dot{\epsilon}_{eq}}{\dot{\epsilon}_{eq}^0} \right) \right] \left[ 1 - d_5 \left( \frac{T - T_0}{T_M - T_0} \right) \right]; \quad (2.84)$$

is the equivalent strain at the damage initiation,  $p$  is the hydrostatic pressure,  $\sigma_{eq}$  is the equivalent stress,  $\dot{\epsilon}_{eq}$  is the equivalent strain rate,  $\dot{\epsilon}_{eq}^0$  is the reference strain rate,  $T$  is the material temperature,  $T_0$  is the reference temperature,  $T_M$  is the material melting temperature, and  $d_i$  ( $i = 1, \dots, 5$ ) are material constants.

The damage evolution (line B–F) can be characterized by the scalar stiffness degradation,  $D$ , which is equal to zero at the damage initiation (point B) and is equal to one at the theoretical final fracture (point F). This parameter can be computed by the expression:

$$D = \frac{\int_0^{u_{eq}^P} \sigma_{eq} du_{eq}^P}{G_f}; \quad (2.85a)$$

for the exponential damage zone, and by the expression:

$$D = 1 - \exp \left( - \int_0^{u_{eq}^p} \frac{\sigma_{eq}}{G_f} du_{eq}^p \right); \quad (2.85b)$$

for the linear damage zone. In both equations,  $u_{eq}^p$  is the equivalent plastic displacement and  $G_f$  is the Hillerborg's fracture energy:

$$G_f = \int_0^{u_{eq}^p} \sigma_{eq} du_{eq}^p. \quad (2.86)$$

The effectiveness of all these models varies notably under different conditions and depends on empirical constant whose experimental determination imposes serious constraints to their use. However, successful application of these approaches has been done in the area of manufacturing FEM-based processes modeling.

## References

- P.J. Arrazola, T. Özel, Investigations on the effects of friction modeling in finite element simulation of machining. *Int. J. Mech. Sci.* **52**, 31–42 (2010). doi:[10.1016/j.ijmecsci.2009.10.001](https://doi.org/10.1016/j.ijmecsci.2009.10.001)
- K.-J. Bathe, *Finite Element Procedures* (Prentice Hall, Upper Saddle River, 1996)
- J. Brocail, M. Watremez, L. Dubar, Identification of a friction model for modelling of orthogonal cutting. *Int. J. Mach. Tools Manuf.* **50**, 807–814 (2010). doi:[10.1016/j.ijmachtools.2010.05.003](https://doi.org/10.1016/j.ijmachtools.2010.05.003)
- J. Chakrabarty, *Theory of Plasticity*, 3rd edn. (Elsevier Butterworth-Heinemann, Oxford, 2006)
- P.M. Dixit, U.S. Dixit, *Modeling of Metal Forming and Machining Processes by Finite Element and Soft Computing Methods* (Springer, London, 2008)
- U.S. Dixit, S.N. Joshi, J.P. Davim, Incorporation of material behavior in modeling of metal forming and machining processes: A review. *Mater. Des.* **32**, 3655–3670 (2011). doi:[10.1016/j.matdes.2011.03.049](https://doi.org/10.1016/j.matdes.2011.03.049)
- L. Filice, F. Micari, S. Rizzuti, D. Umbrello, A critical analysis on the friction modelling in orthogonal machining. *Int. J. Mach. Tools Manuf.* **47**, 709–714 (2007). doi:[10.1016/j.ijmachtools.2006.05.007](https://doi.org/10.1016/j.ijmachtools.2006.05.007)
- B.P.P.A. Gouveia, J.M.C. Rodrigues, P.A.F. Martins, Ductile fracture in metalworking: experimental and theoretical research. *J. Mater. Process. Tech.* **101**, 52–63 (2000). doi:[10.1016/S0924-0136\(99\)00449-5](https://doi.org/10.1016/S0924-0136(99)00449-5)
- W. Grzesik, Determination of temperature distribution in the cutting zone using hybrid analytical-FEM technique. *Int. J. Mach. Tools Manuf.* **46**, 651–658 (2006). doi:[10.1016/j.ijmachtools.2005.07.009](https://doi.org/10.1016/j.ijmachtools.2005.07.009)
- W. Han, B.D. Reddy, *Plasticity: Mathematical Theory and Numerical Analysis* (Springer, New York, 1999)
- S.P.F.C. Jasper, J.H. Dautzenberg, Material behaviour in conditions similar to metal cutting: flow stress in the primary shear zone. *J. Mater. Process. Tech.* **122**, 322–330 (2002). doi:[10.1016/S0924-0136\(01\)01228-6](https://doi.org/10.1016/S0924-0136(01)01228-6)



- D.I. Lalwani, N.K. Mehta, P.K. Jain, Extension of Oxley's predictive machining theory for Johnson and Cook flow stress model. *J. Mater. Process. Tech.* **209**, 5305–5312 (2009). doi:[10.1016/j.jmatprotec.2009.03.020](https://doi.org/10.1016/j.jmatprotec.2009.03.020)
- K. Li, X.-L. Gao, J.W. Sutherland, Finite element simulation of the orthogonal metal cutting process for qualitative understanding of the effects of crater wear on the chip formation process. *J. Mater. Process. Tech.* **127**, 309–324 (2002). doi:[10.1016/S0924-0136\(02\)00281-9](https://doi.org/10.1016/S0924-0136(02)00281-9)
- G.R. Liu, S.S. Quek, *The Finite Element Method: A Practical Course* (Butterworth-Heinemann, Burlington, 2003)
- A.G. Mamalis, A.S. Branis, D.E. Manolacos, Modelling of precision hard cutting using implicit finite element methods. *J. Mater. Process. Tech.* **123**, 464–475 (2002). doi:[10.1016/S0924-0136\(02\)00133-4](https://doi.org/10.1016/S0924-0136(02)00133-4)
- M. Mohammadpour, M.R. Razfar, R.J. Saffar, Numerical investigating the effect of machining parameters on residual stresses in orthogonal cutting. *Simul. Model Pract. Theory* **18**, 378–389 (2010). doi:[10.1016/j.simpat.2009.12.004](https://doi.org/10.1016/j.simpat.2009.12.004)
- L. Olovsson, L. Nilsson, K. Simonsson, An ALE formulation for the solution of two-dimensional metal cutting problems. *Comput. Struct.* **72**, 497–507 (1999)
- T. Özel, E. Zeren, Determination of work material flow stress and friction for FEA of machining using orthogonal cutting tests. *J. Mater. Process. Tech.* **153–154**, 1019–1025 (2004). doi:[10.1016/j.jmatprotec.2004.04.162](https://doi.org/10.1016/j.jmatprotec.2004.04.162)
- O. Pantalé, J.-L. Bacaria, O. Dalverny, R. Rakotomalala, S. Caperaa, 2D and 3D numerical models of metal cutting with damage effects. *Comput. Method Appl. M.* **193**, 4383–4399 (2004). doi:[10.1016/j.cma.2003.12.062](https://doi.org/10.1016/j.cma.2003.12.062)
- A. Pramanik, L.C. Zhang, J.A. Arsecularatne, An FEM investigation into the behavior of metal matrix composites: Tool–particle interaction during orthogonal cutting. *Int. J. Mach. Tools Manuf.* **47**, 1497–1506 (2007). doi:[10.1016/j.ijmachtools.2006.12.004](https://doi.org/10.1016/j.ijmachtools.2006.12.004)
- J. Rech, C. Claudin, E. D'Eramo, Identification of a friction model: Application to the context of dry cutting of an AISI 1045 annealed steel with a TiN-coated carbide tool. *Tribol. Int.* **42**, 738–744 (2009). doi:[10.1016/j.triboint.2008.10.007](https://doi.org/10.1016/j.triboint.2008.10.007)
- P.A.R. Rosa, O. Kolednik, P.A.F. Martins, A.G. Atkins, The transient beginning to machining and the transition to steady-state cutting. *Int. J. Mach. Tools Manuf.* **47**, 1904–1915 (2007). doi:[10.1016/j.ijmachtools.2007.03.005](https://doi.org/10.1016/j.ijmachtools.2007.03.005)
- A. Shabana, *Computational Continuum Mechanics* (Cambridge University Press, Cambridge, 2008)
- C. Shet, X. Deng, Residual stresses and strains in orthogonal metal cutting. *Int. J. Mach. Tools Manuf.* **43**, 573–587 (2003). doi:[10.1016/S0890-6955\(03\)00018-X](https://doi.org/10.1016/S0890-6955(03)00018-X)
- D. Umbrello, Finite element simulation of conventional and high speed machining of Ti6Al4V alloy. *J. Mater. Process. Tech.* **196**, 79–87 (2008). doi:[10.1016/j.jmatprotec.2007.05.007](https://doi.org/10.1016/j.jmatprotec.2007.05.007)
- M.R. Vaziri, M. Salimi, M. Mashayekhi, Evaluation of chip formation simulation models for material separation in the presence of damage models. *Simul. Model Pract. Theory* **19**, 718–733 (2011). doi:[10.1016/j.simpat.2010.09.006](https://doi.org/10.1016/j.simpat.2010.09.006)
- P. Wriggers, *Nonlinear Finite Element Methods* (Springer, Berlin, 2008)
- Y.C. Zhang, T. Mabrouki, D. Nelias, Y.D. Gong, Chip formation in orthogonal cutting considering interface limiting shear stress and damage evolution based on fracture energy approach. *Finite Elem. Anal. Des.* **47**, 850–863 (2011). doi:[10.1016/j.finel.2011.02.016](https://doi.org/10.1016/j.finel.2011.02.016)
- O.C. Zienkiewicz, R.L. Taylor, *The Finite Element Method: The Basis* (Butterworth-Heinemann, Oxford, 2000)

Hybrid Modeling and Optimization of Manufacturing  
Combining Artificial Intelligence and Finite Element  
Method

Quiza, R.; López-Armas, O.; Davim, J.P.

2012, VIII, 95 p. 67 illus., Softcover

ISBN: 978-3-642-28084-9